68th International Astronautical Congress 2017, Adelaide, Australia, 25-29 September 2017

IAC-17-A6.2.8

DRAG AND SOLAR SAIL DEORBITING: RE-ENTRY TIME VERSUS CUMULATIVE COLLISION PROBABILITY

Camilla Colombo[1], Alessandro Rossi[2], Florio Dalla Vedova[3], Vitali Braun[4], Benjamin BastidaVirgili[4], Holger Krag[4].

[1] Politecnico di Milano, Dep. of Aerospace Science and Technology, Milano, Italy; camilla.colombo@polimi.it
[2] IFAC-CNR, Sesto Fiorentino, Italy; a.rossi@ifac.cnr.it
[3] LuxSpace, Luxembourg; dallavedova@luxspace.lu
[4] European Space Agency, ESOC, Darmstandt, Germany

Solar and drag sailing have been proposed as passive end-of-life deorbiting methods, and technological demonstrators are under development. For orbit above 800 km altitude solar radiation pressure can be exploited for increasing the orbit eccentricity until the perigee enters the drag region until final re-entry. The performance of the sailing strategy is determined by four parameters: the required effective area-to-mass ratio to deorbit the spacecraft, which determine the sail size given the satellite's mass, the time to deorbit and the augmented collision probability caused on and by the sail through its passage in the Low Earth Orbit protected region densely populated by space debris. In this paper we assess the sail dimension with respect to the augmented collision risk depending on the sail area and the deorbiting time.

I. INTRODUCTION

Solar and drag sailing have been proposed as passive end-of-life deorbiting methods, and technological demonstrators are under development (see Table 1).

Drag sailing is of benefit for end-of-life disposal of small to medium satellites from orbits of altitude up to 1000 km [1]. Further outside this orbit range, a region extending from high Low-Earth Orbit (LEO) (i.e. 1000 km) up to about 13,000 km, can be identified where solar sailing is of interest [3][2].

In the drag dominated regime the required area-to-mass-ratio for a sail spacecraft is primarily dependant on the semi-major axis, growing exponentially with increasing altitude. In the solar radiation pressure dominated regime, the required area-to-mass ratio strongly depends on both semi-major axis and inclination of the initial orbit. The deorbiting phase, at least in the first phase, is achieved on an elliptical orbit, not a circular orbit like in the case of drag sail with inward deorbiting.

The performance of the sailing strategy is determined by four parameters: the required effective area-to-mass ratio to deorbit the spacecraft, which determine the sail size given the satellite's mass, the time to deorbit and the augmented collision probability caused on and by the sail through its passage in the LEO protected region densely populated by space debris [4]. During deorbiting the satellite passes through the debris environment. The cumulative collision risk can be quantified as a function of the collisional cross-section present in orbit and the time of exposure of this cross-section to the flux of debris present in the environment [5]. While in the drag dominated region is expected that the cumulative collision probability during deorbit does not change if a sail is used, this assumption may not hold if the deorbit exploits the build-up of the eccentricity to reach higher-density regions. A past work by Lücking et al. [6] showed the interaction of the de-orbiting strategy with the debris environment by computing the cumulative collision probability using the standard NASA break-up model [7].

In [6] six test scenarios were chosen: three spacecraft in Sun-synchronous LEO and three spacecraft in Medium Earth Orbit (MEO) at different inclinations. For LEO the Sun Synchronous Orbit (SSO) cases were chosen, as these orbital regimes are among the most congested and consequently at the highest risk of debris collision. The three MEO cases were chosen in such a way as to perform the manoeuvres with a small area-to-mass-ratio as possible while showing a large range of different orbit types. The study showed the cumulative collision risk for these six cases showing that this is driven not only by the area of the sail but also on the orbit evolution, indeed a solar or drag sail have substantially different orbit evolution, therefore they interact with the space debris environment differently. Moreover, it has to be taken into account that the deorbiting time with a sail or tether decreases with respect to the standard spacecraft deorbiting time. This is the aim of the current work.

In this paper we first compute the required sail area to deorbit from a wide range of orbital regions, from LEO to MEO. An assessment of the applicability of passive de-orbit devices to the disposal phase of the satellites is performed. A wide domain of initial circular orbits is defined in terms of semi-major axis, inclination, right ascension of the ascending node and anomaly of the perigee. For each initial orbit the analysis aims at determining whether the satellite starting from each operational orbit can be de-orbited with an area augmentation device (i.e. sail or balloon). For a selected number of these solutions the cumulative collision probability with the Space Debris Model SDM evolution tool [8]. A trade-off between the time to deorbit and the cumulative collision risk will be performed to design the sail size so that the deorbiting will have the minimum effect onto the debris population. Based on the launch trends in LEO to MEO for the past 5 years, an assessment of the application of deorbit sailing to future nanosatellites will be also made.

The paper is organised as follow: Section II discussed the current and planned low-mass satellite missions in the period 2010-2016. Section III presents an extended analysis (with respect to [2][3][4]) on the applicability of drag and solar sails for end-of-life deorbiting, In particular different desired deorbiting time and different initial condition in right ascension of the ascending node are considered. The effect of drag on top of solar radiation pressure is also considered in Section IV. Finally, to assess the effect of the deorbiting device on the space debris environment, the cumulative collision probability of selected deorbiting scenarios is calculated in Section V.

Table 1. Current drag sail projects.

c_R	Sidelenght [m]	Area [m^2]	s/c mass [kg]	$c_R A/m$ [m^2/kg]	Remarks
0.9	21.21	450	3500	0.1157	Max DGNC boom
0.9	15	225	3500	0.0579	Max TRL in Europe within 2025 (FDV estimate)
0.9	21.21	450	1000	0.4050	Max DGNC boom
0.9	15	225	1000	0.2025	Max TRL 8 in Europe within 225 (FDV estimate)
0.9	5	25	1000	0.2025	DGNC “normal case” flat
0.9	5	25	100	0.0225	Microsats (high end)
0.9	5	25	10	0.2250	Microsats (low end)
0.9	3.16	10	3.5	2.5714	Nanosail-D2 (3U Cubesat)

0.9	2.00	4	3.75	0.9600	Canada (3U Cubesat)
0.9	1.5	2.25	1	2.0250	Max A, probable for 1U CubeSat

II. CURRENT AND PLANNED LOW-MASS SATELLITE MISSIONS

This analysis focuses on satellites with mass below 1000 kg (satellite classes: nano 1–10 kg, micro 10–100 kg, mini 100–1000 kg), to reflect the fact that that objects with larger mass tend to have a propulsion system and thus are unlikely to require passive de-orbit means. A survey of all satellites launched over the years [2010, 2016] was performed to analyse the number of launches per year to various orbital regions and to identify the objects that will need a de-orbiting/disposal solution. These evolutions are quantitatively presented in Table 2 together with their basic statistical characterisations. The total number of launches per year is represented in Fig. 1 and has an average of 83 launches per year. Temporal extrapolations shall however also consider the announced advent of large, even "mega" constellations. As most of these large-constellations already started to be implemented in the last 2-3 years, their rates of satellites injections in space have already be accounted in Table 2 and Fig. 1. The mega-constellations not yet implemented have not been included instead (i.e. Boeing, SpaceX and OneWeb). Fig. 2 show, for each satellite mass category, the recent evolution of perigees in LEO at injection. Such information will be used later on to identify and extrapolate the LEO orbital regions that could be occupied by future launches. Over the launch period considered (i.e. [2010, 2016]), LEO satellites in the range:

-]0; 1] kg class present a decreasing trend for maximal and average perigee altitudes of injection. It has to be noted that in 2016 very close values of minimum/average/maximum perigee altitudes to the International Space Station and the Chinese *Tiangong-1* and *-2* altitudes.
-]1; 10] kg class also present a decreasing trend for maximal and average perigee altitudes. In this case a larger spread can be seen for the injection perigee altitude, i.e. 215/450/661 km.
-]10, 100] kg class present a rather stable trend for average, and a recent decreasing trend for maximal perigee altitudes. In 2016 a spread of minimum/average/maximum perigee altitudes similar to the one observed for the previous]1, 10] kg class can be seen (here: 287/521/700 km).
-]100, 1000] kg class present a decreasing trend for average, and a stable trend for maximal perigee altitudes.

Table 2. Evolution of satellite launches over the years [2010, 2016].

Objects to Deorbit												
	avg	std	min	max	**2016**	**2015**	**2014**	**2013**	**2012**	**2011**	**2010**
from LEO:	126	55	63	192	154	175	192	157	75	69	63
from LEO (not ISS&TG):	97	34	63	153	101	115	117	153	67	66	63
from LEO (SSO):	55	24	28	84	76	51	84	78	28	38	28
from LEO (ISS&TG):	29	32	0	75	53	60	75	4	8	3	0
from HEO/EEO:	4	2	0	6	1	6	5	4	4	5	0
from MEO:	9	4	3	15	10	11	15	6	3	9	7
Mass to Deorbit (in tons)											
	avg	std	min	max	**2016**	**2015**	**2014**	**2013**	**2012**	**2011**	**2010**
from LEO:	65.2	16.5	47.5	95.5	54.8	66.6	69.6	72.1	47.5	95.5	50.2
from LEO (not ISS&TG):	65.0	16.5	47.3	95.5	54.5	66.3	69.3	72.1	47.3	95.5	50.2
from LEO (SSO):	30.7	7.4	17.6	36.5	34.1	32.3	35.4	36.5	22.7	36.0	17.6
from LEO (ISS&TG):	0.18	0.15	0.00	0.38	0.28	0.30	0.38	0.01	0.19	0.07	0.00
from HEO/EEO:	7.3	7.7	0.0	22.5	0.4	6.0	22.5	7.5	4.4	10.5	0.0
from MEO:	9.7	4.3	3.0	16.4	9.9	11.3	16.4	5.8	3.0	11.0	10.4
Objects Mass Distribution for LEO-PR											
Nb of objects which mass is:	avg	std	min	max	**2016**	**2015**	**2014**	**2013**	**2012**	**2011**	**2010**
= 0 kg (i.e. mass unknown)	7	2	5	10	9	10	6	10	5	5	5
in]0 ; 1] kg	15	13	3	43	8	18	14	43	15	6	3
in]1 ; 10] kg	56	49	6	126	74	109	126	46	10	6	18
in]10 ; 100] kg	16	8	4	28	22	19	28	15	14	12	4
in]100 ; 1000] kg	26	3	22	30	24	26	26	30	23	29	22
> 1,000 kg	31	4	24	35	29	34	35	29	24	35	28

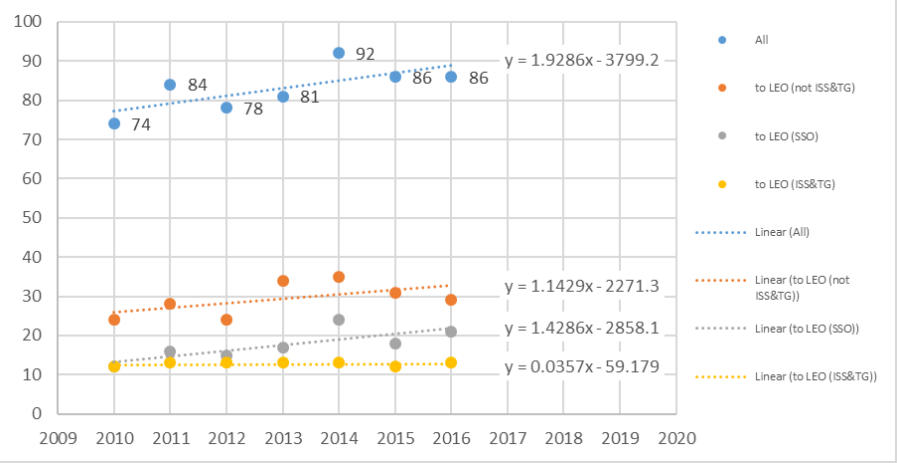

Fig. 1. Evolution of number of launches per year over the period [2010, 2016].

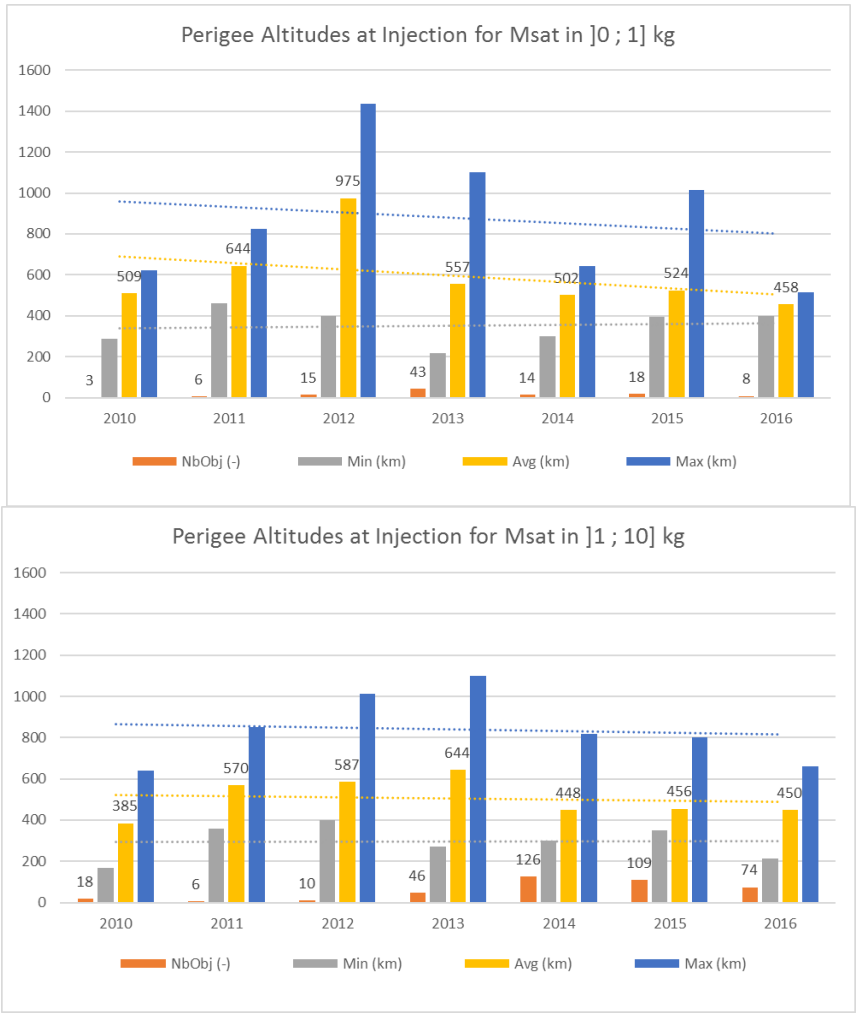

Fig. 2. Recent evolutions of numbers and minimum/average/maximum perigee altitudes at injections in LEO for]0 ; 1] and]1 ; 10] kg satellites.

III. APPLICABILITY OF SOLAR AND DRAG SAILS FOR END-OF-LIFE DEORBITING

From the orbital dynamic point of view, deorbiting can be obtained by decreasing the semi major axis of the orbit *a* and therefore spiralling down, if the initial orbit is a circular one, or alternatively can be obtained by increasing the eccentricity *e* of the orbit [4]. This can be clearly seen from the variational equation of the orbit perigee r_p:

$$\frac{dr_p}{dt} = \frac{da}{dt}(1-e) + a\left(1-\frac{de}{dt}\right)$$

These two different strategies will be explained in section III.I and III.II respectively.

III.I. Inward spiralling deorbiting

The most common strategy for deorbiting via a sail is inward spiralling deorbiting. This is the strategy used by drag sails and aims at augmenting the cross area of the satellite so that the effect of the atmospheric drag can be exploited to decrease the semi-major axis as the acceleration due to aerodynamic drag is always against the velocity vector [4]:

$$\frac{da}{dt} = \frac{2a^2 v}{\mu_{\text{Earth}}}\left\langle \mathbf{a}_{\text{drag}} \cdot \hat{\mathbf{v}} \right\rangle$$

where v is the spacecraft velocity, μ_{Earth} the gravitational parameter of the Earth and $\left\langle \mathbf{a}_{\text{drag}} \cdot \hat{\mathbf{v}} \right\rangle$ represents the scalar

product between the perturbing acceleration induced by aerodynamic drag and the velocity vector of the spacecraft. Several studies in the past have assessed the required sail area to deorbiting via the deployment of a drag sail. As an example, [9] gives for a given satellite mass and its initial de-orbit altitude the drag sail size (i.e. side length of the square, flat sail) needed to de-orbit (while passively tumbling) the satellite in 25 years. Also Janovsky et al. [1] gives the orbital lifetime of satellites as function of their area-to-mass ratio.

Fig. 3. Required drag sail side length to deorbit within 25 years for various satellite masses and initial de-orbit altitudes.

The same effect of inward deorbiting can be also obtained well outside the atmosphere via active attitude control solar sailing. The solar sailing strategy proposed by Borja and Tun [11] aims at maximising the cross area of the sail perpendicular to the spacecraft-Sun direction when the spacecraft is moving towards the Sun, while the sail area is minimised when the spacecraft is flying away from the Sun. In this way the semi-major axis and thus the energy of the orbit is continuously decreased. The osculating variation of the semi-major axis a is:

$$\frac{da}{dt}=\frac{2a^2v}{\mu_{\text{Earth}}}\left\langle \mathbf{a}_{\text{SRP, max}}\cdot\hat{\mathbf{v}}\right\rangle$$

where $\left\langle \mathbf{a}_{\text{SRP, max}}\cdot\hat{\mathbf{v}}\right\rangle$ is the component of the acceleration in the tangential direction. In the half of the orbit where this product term would be negative, the sail is oriented facing the Sun, in the other case the normal to the sail is oriented perpendicular to the spacecraft-Sun direction so that the acceleration caused by the sail is zero. Therefore, the active control on the sail will be:

$$\begin{cases}\text{if} & \left\langle \hat{\mathbf{r}}_{\text{Sun-s/c}}\cdot\hat{\mathbf{v}}\right\rangle<0 \quad \mathbf{a}_{\text{SRP, act}}=p_{\text{SR}}c_{\text{R}}A_{\text{Sun}}/m\,\hat{\mathbf{r}}_{\text{Sun-s/c}}\\ \text{elseif} & \left\langle \hat{\mathbf{r}}_{\text{Sun-s/c}}\cdot\hat{\mathbf{v}}\right\rangle>=0 \quad \mathbf{a}_{\text{SRP, act}}=\mathbf{0}\end{cases}$$

Active solar sailing techniques was compared to the passive solar sailing technique in [4] to determine the most efficient deorbiting strategy under a maximum deorbiting time constraint; results showed that passive sailing should be preferred in most of the cases. Therefore, in this study we will only focus on this second strategy and we will couple solar sailing with drag sailing for optimising the re-entry condition (minimum sail size, minimum deorbiting time, and minimum cumulative collision risk).

III.II. Outward elliptical deorbiting

We will here focus on passive attitude control solar sailing also called here outward deorbiting. As already explained, the deorbiting is obtained by increasing the eccentricity of the orbit, thus decreasing the orbit perigee. So the deorbiting phase, at least in the first phase, is achieved on an elliptical orbit, not a circular orbit like in the case inward deorbiting. In this case the decrease of the perigee is attained by acting on the variation of the eccentricity [4]:

$$\frac{de}{dt}=\frac{1}{v}\left(2\left(e+\cos f\right)\left\langle \mathbf{a}_{\text{SRP, max}}\cdot\hat{\mathbf{v}}\right\rangle\right)-\frac{r}{a}\sin f\left\langle \mathbf{a}_{\text{SRP, max}}\cdot\hat{\mathbf{n}}\right\rangle$$

The effect can be easily explained by considering, for simplicity a planar orbit.

We define $\phi=\Omega+\omega-\left(\lambda_{\text{Sun}}+\pi\right)$ as the angle between the Sun radiation and the perigee of the orbit. This angle is the one that governs the fact that the eccentricity in increasing or decreasing. Starting from a circular orbit, the effect of solar radiation pressure is to naturally increase the eccentricity until a maximum value. After this the orientation of the perigee with respect to the Sun changes and the eccentricity starts to decrease again. Lücking et al. [3][2] proposed to exploit this natural dynamics for achieving re-entry via a solar sail. The sail area-to-mass is chosen so that, the maximum eccentricity attained during the orbit evolution is equal to the critical eccentricity $e_{\text{crit}}=1-\left(R_{\text{E}}+h_{\text{p,drag}}\right)/a$ so that the spacecraft re-enter deeply in the drag dominated region.

After that the sail acts as a drag sail, therefore the orbit circularises again while the semi-major axis decrease, until final re-entry. Depending on the initial semi-major axis and inclination of the initial circular orbit, the initial phase dominated by Solar Radiation Pressure (SRP) is different by the effect is always to increase the eccentricity of the orbit. This can be seen in [3] that shows, for different semi-major axis, the path followed by the deorbiting spacecraft under the effect of solar radiation pressure and Earth's oblateness.

The aim of this section is to calculate the sail requirements for deorbiting through passive sailing. This will be done as in [3][2] by computing the minimum effective area-to-mass ratio $\left(c_R A_{sail}\right)/m$ that causes the eccentricity to grow up to the critical value (eccentricity value such as the orbit perigee is well inside the Earth's atmosphere, i.e. 120 km altitude). The effective area-to-mass requirement depends on the desired maximum allowed deorbiting time. In this phase, initial circular orbit will be considered for various inclination and semi-major axis in the LEO and MEO region. The choice of considering only circular orbit is justified by the distribution of current spacecraft in LEO.

The sail requirements dependence on the initial orbit eccentricity and right ascension of the ascending node will be also analysed. A wide domain of initial orbits was defined in terms of semi-major axis, inclination, right ascension of the ascending node and anomaly of the perigee.

For each initial orbit an optimisation procedure is employed to calculate the minimum effective area to mass ratio required for deorbiting in a given deorbiting time. As all the initial orbits from LEO to MEO want to be assessed, a fast tool is needed, to compute the orbit evolution depending on the initial orbit for different de-orbiting strategies. For this analysis, the Planetary Orbital Dynamics (PlanODyn) suite is used [12]. As in this analysis we want to calculate a preliminary value of $\left(c_R A_{sail}\right)/m$ on a wide domain of semi-major axis and inclination, the simulation is performed only considering SRP and J_2. This indeed is the most conservative case as the whole deorbiting is achieved only with SRP eccentricity growth. Once drag is also considered its effect is the one of progressively decreasing the semi-major axis and, as this effect will superimpose to the effect of SRP + J_2. As it will be shown later, the deorbiting will takes place in a longer time, but a lower value of sail would be sufficient. In any case, while this analysis is to find a preliminary value of the sail area, in Section IV, the effect of drag will be taken into account.

Fig. 4 shows in colour the effective area-to-mass ratio in [m^2/kg] to de-orbit from circular orbit with sail passive mode strategy considering a maximum deorbiting time of one year. The required $\left(c_R A_{sail}\right)/m$ is calculated for different initial orientation with respect to the Sun, i.e. different initial Ω. The left column shows the effective area-to-mass ratio requirement needed to deorbit in less than a year; in the right column the results are bounded at a maximum value of 30 m^2/kg. The aim of this analysis is to show that the solar sail requirements strongly depends on the initial operational orbit. There are some initial conditions, for semi-major axis from 800 to 14000 km that require a small value of the sail to achieve deorbit in a very short time. The reason for this behaviour is explained in Lücking et al. [2]; indeed, depending on the orbit *a* and the inclination *i*, a different behaviour in the orbit evolution among the three shown in [2] is followed during re-entry, due to the interaction between the J_2 effect and solar radiation pressure. Increasing the semi-major axis, the orbit behaviour switches from the phase space characterised by the existence of an equilibrium in correspondence to $\phi = 0$ to the phase space characterised by an equilibrium in correspondence to $\phi = 0$ for very

high initial eccentricity and two equilibria in correspondence of $\phi = \pi$ [13]. This happens via a bifurcating phase space behaviour; the switching to different behaviour depending on the semi-major axis of an initial planar orbit is shown [2]. When the re-entry behaviour takes place starting from e = 0 and following the phase space line that passes through the hyperbolic equilibrium point, the required sail area is the minimum one, but the time to deorbit could in theory go to infinity [2]. This analysis is in perfect agreement with the analysis of resonances in the LEO region performed by Alessi et al. using a simplified analytical method and validated via Fourier analysis ref. Now, looking closer in the orbital region where the J_2 perturbation is dominant, the effective area-to-mass ratio required to deorbit sharply decreases with increasing altitude and inclination. In the SRP dominant orbital configuration, the area-to-mass ratio required increase with increasing inclination and with increasing altitude. Except for high inclination (above 45°), in which the area-to-mass ratio decrease with increasing altitude. Fig. 4 shows the requirements for LEO orbit and some MEO and focuses on the orbit regions where the requirements in terms of sail size are realisable with current technologies. For the same initial conditions, Fig. 5 shows the corresponding deorbiting time. Note that, as the maximum deorbiting time was set to one year, the conditions corresponding to the minimum area-to-mass ratio takes around one year to deorbit. In the following of this study simulations for longer than one year deorbiting time will be performed as this will allow reducing the sail size. Fig. 5 shows the deorbiting time for the LEO deorbiting cases, all well below one year time.

In Section IV the effect of drag will be included and in Section V some selected test cases from the analysis presented will be used to calculate the cumulative collision probability during re-entry.

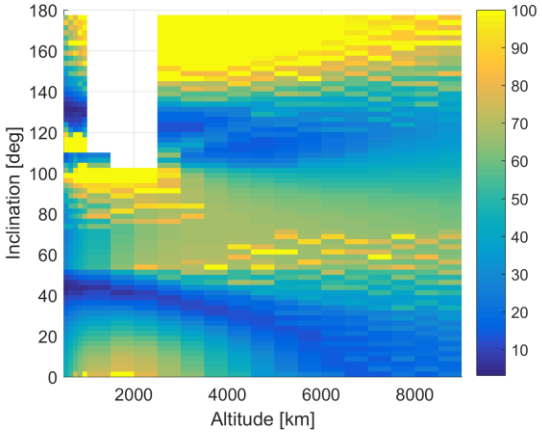

Ω_0 = 0 degrees

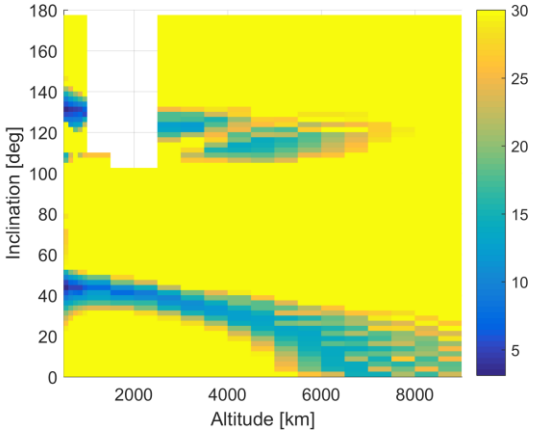

Ω_0 = 0 degrees

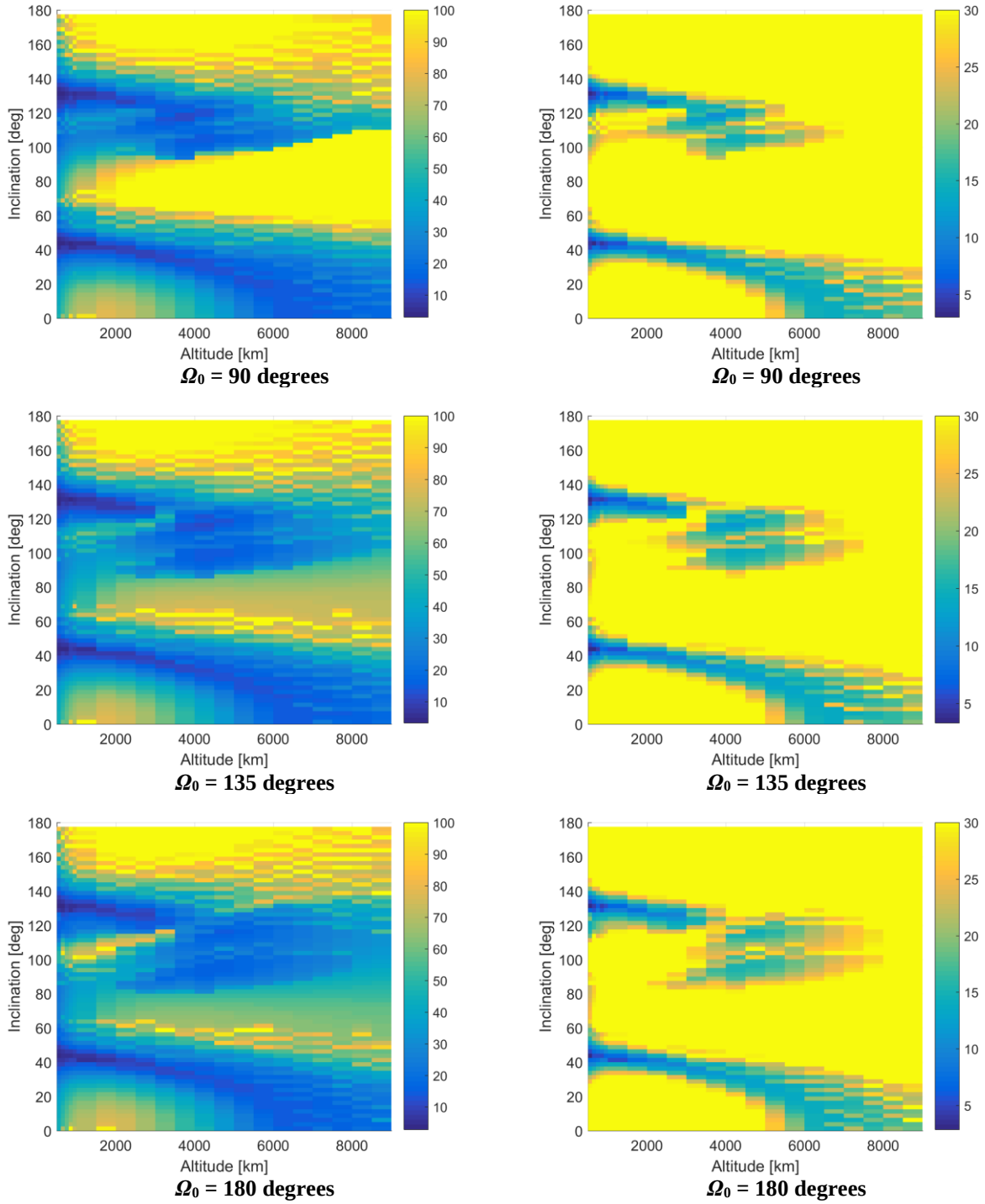

Fig. 4. Effective area-to-mass ratio in [m^2/kg] to de-orbit from circular low Earth orbit and different initial orientation with respect to the Sun, with sail passive mode strategy. (Left) Effective area-to-mass ratio requirements, (Right) Effective area-to-mass ratio requirements with maximum limits set at 30 m^2/kg.

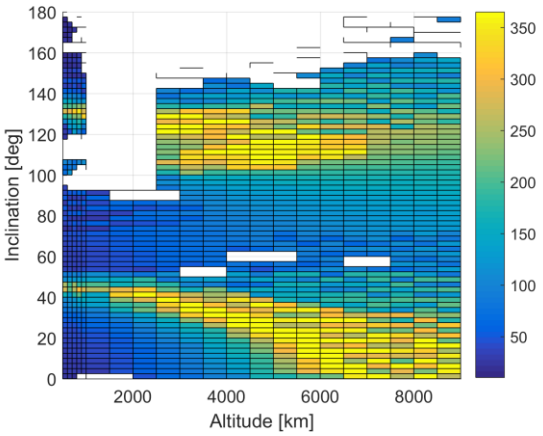

Ω_0 = 0 degrees

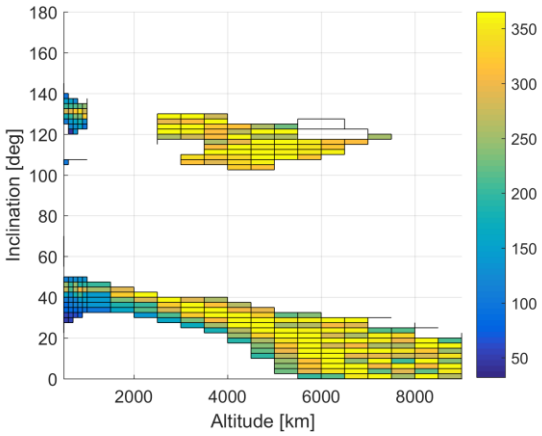

Ω_0 = 0 degrees

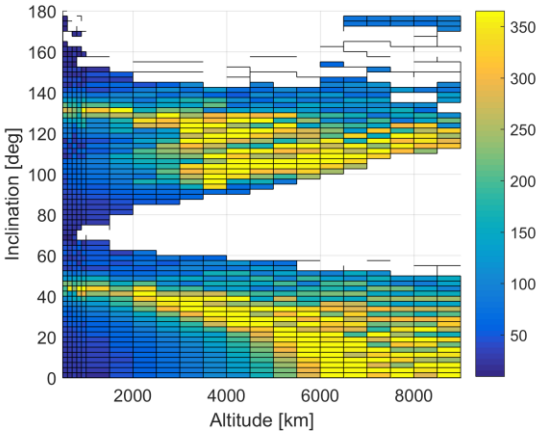

Ω_0 = 90 degrees

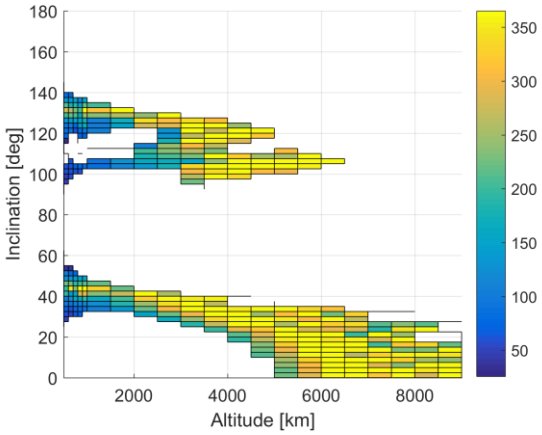

Ω_0 = 90 degrees

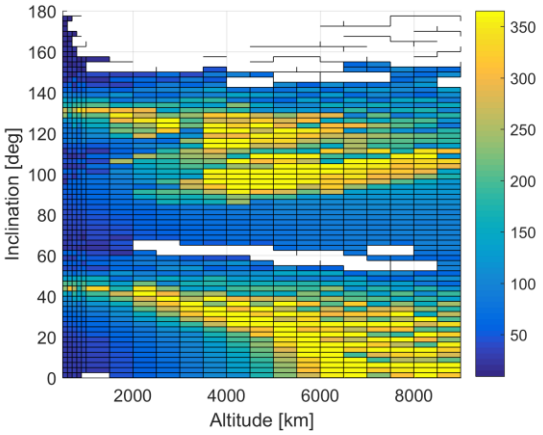

Ω_0 = 135 degrees

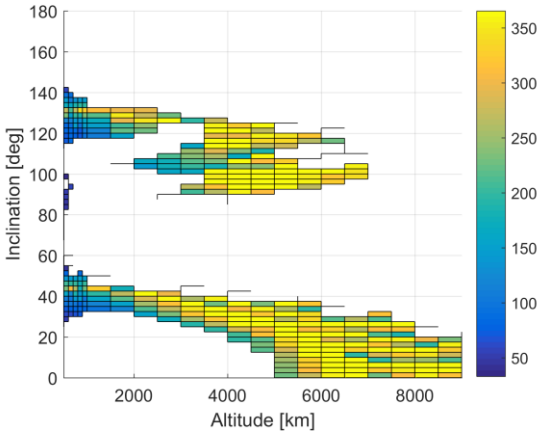

Ω_0 = 135 degrees

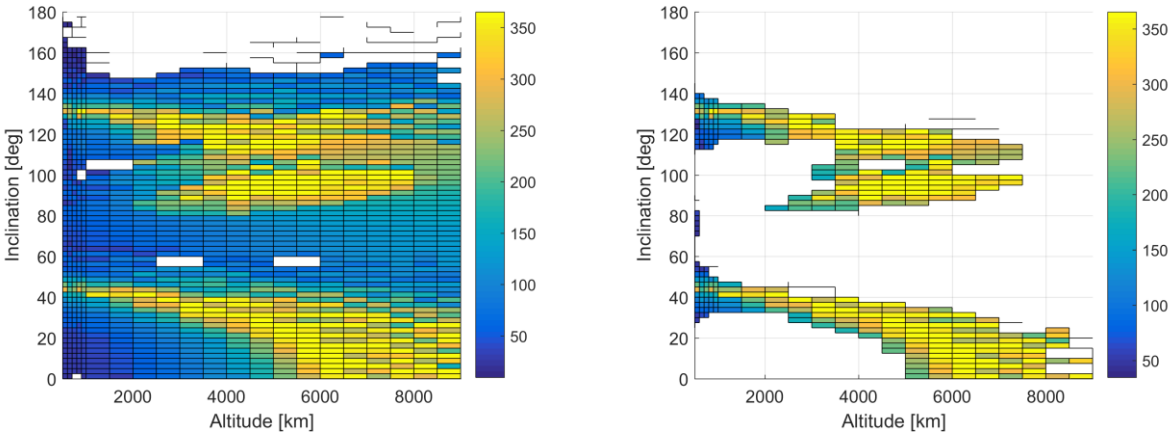

Ω_0 = 180 degrees **Ω_0 = 180 degrees**

Fig. 5. Time to de-orbit from circular orbit and different initial orientation with respect to the Sun, with sail passive mode strategy. (Left) All solutions, (Right) Selected solutions where the effective area-to-mass ratio requirements is below the maximum limits set at 30 m^2/kg.

IV. EFFECT OF ATMOSPHERIC DRAG

The models for the orbit propagation and the analysis of the evolution of the space debris environment were upgraded and a unified atmosphere model, the Jacchia 77 model was selected.

As the aim of this work is to evaluate the additional collision risk due to the sail augmented area, in the case of a de-orbiting device is used, such as solar or drag sails/balloons.

In this section one deorbiting scenario is shown. Rather than selecting different initial orbit for testing the deorbiting, the same operational orbit was adopted for all the test cases, having the following orbital elements: h_0 = 799.9283 km, $e_0 = 10^{-5}$, i_0 = 42.5 deg, Ω_0 = 90 deg, ω_0 = 0 deg and M_0 = 0 deg. Instead, different deorbiting devices were considered, namely drag and solar sail, characterised by three values of area-to-mass ratio: A/m = 4.1943 m^2/kg, half of this value (2.0971 m^2/kg) and a quarter of it (1.0486 m^2/kg). When only drag is exploited for deorbiting the sail material is chosen with $c_D = 2.1$ and $c_R = 0.1$, while, if we want to exploit also the effect of solar radiation pressure, the deployable sail is chosen so that $c_D = 2.1$ and $c_R = 1$. The deorbiting phase was propagated in mean elements by using PlanODyn considering a dynamical model including the zonal terms of the Earth's gravity field J_2 to J_6, solar radiation pressure and drag, considering a fixed $T_{exosphere}$ fixed to 1000 K. Table 3 shows the selected test cases for the calculation of the flux. The first two cases represents a conventional satellite with A/m = 0.012 m^2/kg, the other cases represents the effect of drag or solar sail.

The deorbiting trajectory is represented in Fig. 6 over a time window of 1 year. For the standard spacecraft (scenario 01 and scenario 02) the perigee altitude is decreasing very slowly indeed the deorbiting time is above the maximum limit set for the simulation to 25 years. The scenarios 03 to 09 include the use of a sail on the same spacecraft. In this case, as the initial condition of the operational orbit is chosen, the A/m and the reflectivity and drag coefficients are the parameter that decides the re-entry behaviour. When a sail is deployed the deorbiting takes place in a shorter time of flight. Fig. 6 contains the deorbiting using three sail sizes, corresponding to A/m of 4.1943 m^2/kg (red), half of this value i.e., 2.0971 m^2/kg (green) and a quarter of it i.e. 1.0486 m^2/kg (blue). As expected, the higher the A/m the shorter is the deorbiting. In Fig. 6 the difference between

the deorbiting exploiting the effect of drag only (continuous line) and the deorbiting exploiting the effect of drag and SRP (dashed line) is also highlighted. As shown in [4] the two ways of deorbiting are quite different. The drag only de-orbiting reduces the perigee altitude by reducing the semi-major axis, the SRP enhanced de-orbiting, instead, reduces the orbit perigee by acting on the eccentricity of the orbit. As also drag is presence the evolution of the eccentricity increases in the first phase of the deorbiting and then decrease afterwards. As a net effect in any case, the exploitation of SRP reduces the required time for deorbit with respect to the drag only case.

Table 3. Selected test cases for the calculation of the collision risk.

	Scenario	Area-to-mass ratio [m²/kg]	Perturbation considered	Drag coefficient c_D	Reflectivity coefficient c_R
1	standard s/c	0.012	J_2–J_6, SRP, drag	2.1	0.1
2	standard s/c	0.012	J_2–J_6, SRP, drag	2.1	1
3	S drag sail	1.0486	J_2–J_6, SRP, drag	2.1	0.1
4	S SRP + drag sail	1.0486	J_2–J_6, SRP, drag	2.1	1
5	M drag sail	2.0971	J_2–J_6, SRP, drag	2.1	0.1
6	M SRP + drag sail	2.0971	J_2–J_6, SRP, drag	2.1	1
7	L drag sail	4.1943	J_2–J_6, SRP, drag	2.1	0.1
8	L SRP + drag sail	4.1943	J_2–J_6, SRP, drag	2.1	1
9	L SRP sail	4.1943	J_2–J_6, SRP, no drag	0	1

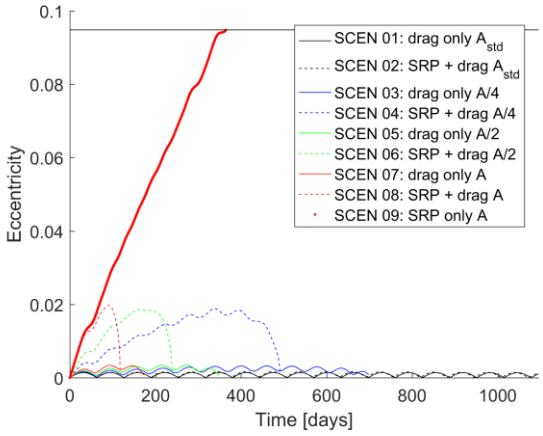

a)

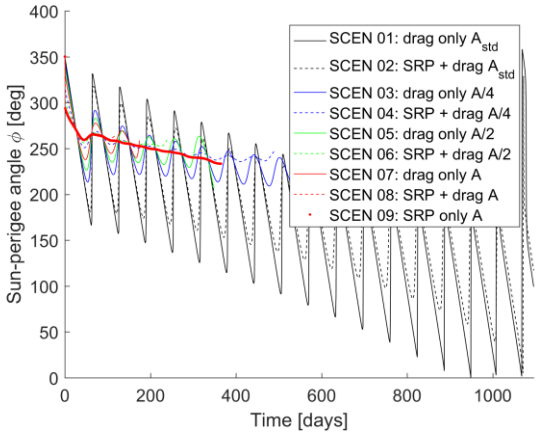

b)

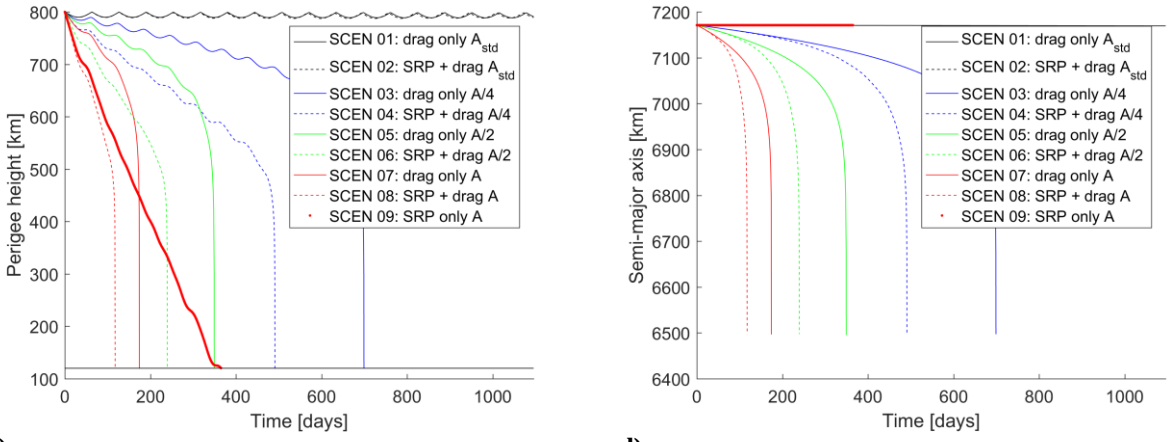

c) **d)**

Fig. 6. Deorbiting trajectory for the selected scenarios: continuous line drag sail only, dashed line drag and solar sail. Evolution of the orbital elements: a) eccentricity, b) Sun-perigee angle, c) perigee altitude, d) semi-major axis.

V. COLLISION RISK WITH AND WITHOUT PASSIVE DE-ORBITING DEVICE

The post-processing module of the Space Debris Model SDM 4.2 is used [8]. A user-defined spacecraft is flown through the debris environment, output from a full run of SDM, and the flux of particles, of variable dimensions, impinging on the target orbit is computed and recorded. The orbit of the "target" deorbiting spacecraft is an external ephemeris file calculated with PlanODyn and passed to SDM with a 1-day step to compute the resulting flux. The simulation setup is as follows:

- The overall debris environment, obtained as output of an SDM simulations of a *business-as-usual* scenario, is used as the background debris population against which a selected target object is flown.
- The orbit of the target objects (i.e. the sail spacecraft) is read from external ephemeris files provided computed by PlanODyn.
- All the orbital crossings between the target and are recorded and the corresponding collision probability is computed using the CUBE algorithm [10].
- For this purpose, CUBE is evaluated with a time-step of 1 day. It is worth remembering that the standard CUBE evaluation time step for an SDM run is 5 days.
- To cumulate statistics, at each evaluation time step, the anomalies of the population objects (i.e., projectiles) are randomised and the CUBE evaluation is performed for the 500 randomised anomalies (resulting in a local Monte Carlo simulation).

For each scenario in Table 3, the collision risk both cumulated over time and "differential", i.e., the collision risk computed for each single epoch (i.e. every day).

Note that, as mentioned e.g. in [5], the mean number of collisions N_c encountered by an object of collision cross-section A, moving through a stationary medium of uniform particle density D, at a constant velocity v, during a propagation time interval Δt is given by:

$$N_c = v D A \Delta t$$

where $F = vD$ is the impact flux (in units of m^{-2} s^{-1}), and $\Phi = F\Delta t$ is the corresponding fluence (in units of m^{-2}). In our plots we chose to show the collision risk (and not the flux) because the former show directly the effect of the actual area of the target object which, in the case of sails, is of paramount importance for our considerations.

As the deorbiting scenarios where selected in based on the value of the *A*/*m*, which is the parameter that affect the deorbiting behaviour, when calculating the number of collisions an area *A* and a mass *m* need to be specified. As the spacecraft masses to be considered in this study should be less than 1000 kg, four values of masses [1, 10, 100, 1000] kg will be considered here.

As a first approximation, let's assume that, given the mass of the spacecraft, the cross area of the sail can be calculated from $atm = A/m$ and from there the length size of the sail is computed $l = \sqrt{atm} \cdot m$, and the equivalent diameter for the calculation of the collision probability is $D_{eq} = \sqrt{2}l$. Note that this diameter is larger than the actual sail size *l*. The spacecraft parameters used for the computation of the collision probability are reported in Table 4.

Table 4. Spacecraft parameters used to calculate the collision probability.

	Scenario	Area-to-mass ratio [m²/kg]	1 kg s/c		10 kg s/c		100 kg s/c		1000 kg s/c	
			Area [m²]	D_{eq} [m]	Area [m²]	D_{eq} [m]	Area [m²]	D_{eq} [m]	Area [m²]	D_{eq} [m]
1	standard s/c	0.012	0.012	0.15	0.12	0.49	1.2	1.55	12	4.899
2	standard s/c	0.012	0.012	0.15	0.12	0.49	1.2	1.55	12	4.899
3	S drag sail	1.0486	1.0486	1.45	10.49	4.58	104.86	14.48	1048.6	45.794
4	S SRP + drag sail	1.0486	1.0486	1.45	10.49	4.58	104.86	14.48	1048.6	45.794
5	M drag sail	2.0971	2.0971	2.05	20.97	6.48	209.71	20.48	2097.1	64.763
6	M SRP + drag sail	2.0971	2.0971	2.05	20.97	6.48	209.71	20.48	2097.1	64.763
7	L drag sail	4.1943	4.1943	2.90	41.94	9.16	419.43	28.96	4194.3	91.589
8	L SRP + drag sail	4.1943	4.1943	2.90	41.94	9.16	419.43	28.96	4194.3	91.589
9	L SRP sail	4.1943	4.1943	2.90	41.94	9.16	419.43	28.96	4194.3	91.589

For the test cases reported in Table 3 and Table 4, Table 5 reports the deorbiting time and the cumulative collision probability during the EOL phase for spacecraft of mass [1, 10, 100] kg. Fig. 7 shows the "differential" collision risk, i.e., the collision risk computed for each single epoch (i.e. every day). Fig. 8, Fig. 9 and Fig. 10 show the collision risk cumulated over time compared over the scenarios 01 to 08. Note that scenario 09 is excluded from these figures as it is a non-physical scenario since the effect of drag is not considered.

The effect of the dimension of the sail can be observed by comparing scenario 01 (no sail), 03 (small sail), 05 (medium sail) and 07 (large sail), where the sail area is progressively increased. When the sail dimension is higher, the deorbiting phase completes in a shorter time, therefore the cumulative collision probability line is steeper. The maximum attained by the cumulative

collision curve is the total cumulative collision probability over the deorbiting. The total cumulative collision probability is also reported in Table 5; note that the total collision probability of scenario 01 and 02 is calculated only considering the trajectory for 25 years. As the spacecraft does not re-entry within 25 years, the actual total collision probability would be higher than the one reported in the table as the spacecraft would spend much longer time in orbit.

It is interesting to observe that the larger is the sail, the lower is the total collision probability as the deorbiting is much faster. If we imagine to reduce the area of the sail until the area-to-mass is the one of a standard satellite (black line in Fig. 8, Fig. 9 and Fig. 10), the slope of the collision probability line is lower but the total collision probability is higher as the spacecraft spend linger time in orbit where the debris population is more dense.

The time of deorbit and cross area do not enter in a simple proportional way in the computation of the total collision probability. This is due to the fact that, by changing the area, the re-entry trajectory changes, therefore the spacecraft spends different interval time at different altitudes where space debris are distributed. So the results of Fig. 8, Fig. 9 and Fig. 10 are dependent not only on the deorbiting time and the cross area, but also on the space debris distribution.

The difference in between using a drag sail only and a drag + solar sail can be observed by comparing scenarios 01, 03, 05, 07, with scenarios 02, 04, 06, 08. In most of the cases the total collision probability for the drag + SRP sail is lower than the total collision probability for the drag only sail as the former deorbit happens on an elliptical path so the spacecraft spends only fraction of the orbit in the most populated region of space debris. One exception is scenario 03 and scenario 04 for the 1 kg spacecraft (see blue line in Fig. 8). It is also important to note that this behaviour may change depending on the initial orbit altitude because, depending on the orbit evolution (circular or elliptical path) the spacecraft will spend a different interval of time in different debris regions.

Table 5. Collision probability for the selected test cases.

	Scenario	Area-to-mass ratio [m^2/kg]	Deorbiting time	Cumulative collision probability		
				1 kg s/c	10 kg s/c	100 kg s/c
1	standard s/c	0.012	Over 25 y	$7.880 \cdot 10^{-8}$	1.149·10–7	$3.646 \cdot 10^{-7}$
2	standard s/c	0.012	Over 25 y	$7.751 \cdot 10^{-8}$	1.142·10–7	$3.677 \cdot 10^{-7}$
3	S drag sail	1.0486	699 days	$2.234 \cdot 10^{-8}$	$1.459 \cdot 10^{-7}$	$1.308 \cdot 10^{-6}$
4	S SRP + drag sail	1.0486	491 days	$2.372 \cdot 10^{-8}$	$1.390 \cdot 10^{-7}$	$1.208 \cdot 10^{-6}$
5	M drag sail	2.0971	349 days	$1.888 \cdot 10^{-8}$	$1.410 \cdot 10^{-7}$	$1.311 \cdot 10^{-6}$
6	M SRP + drag sail	2.0971	239 days	$1.719 \cdot 10^{-8}$	$1.216 \cdot 10^{-7}$	$1.113 \cdot 10^{-6}$
7	L drag sail	4.1943	174 days	$1.639 \cdot 10^{-8}$	$1.350 \cdot 10^{-7}$	$1.282 \cdot 10^{-6}$
8	L SRP + drag sail	4.1943	118 days	$1.432 \cdot 10^{-8}$	$1.139 \cdot 10^{-7}$	$1.072 \cdot 10^{-6}$
9	L SRP sail	4.1943	365 days	$3.081 \cdot 10^{-8}$	$2.372 \cdot 10^{-7}$	$2.214 \cdot 10^{-6}$

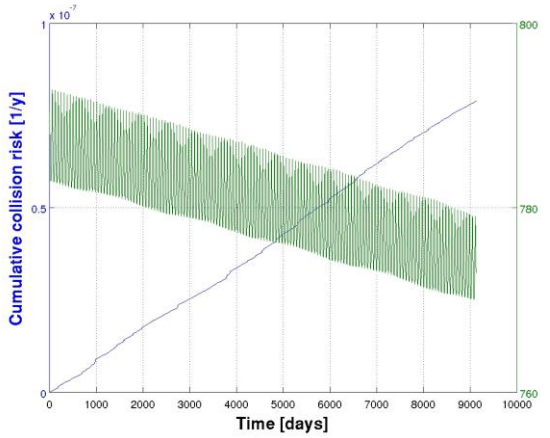

a)

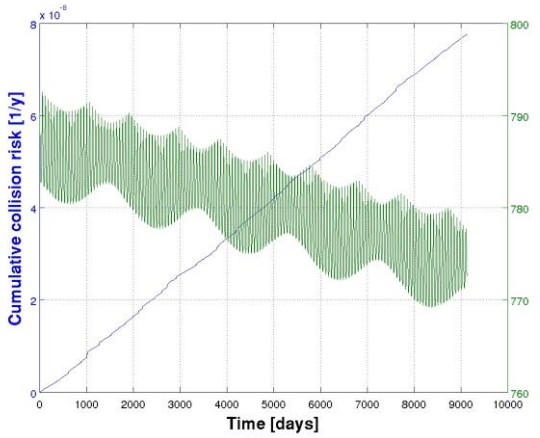

b)

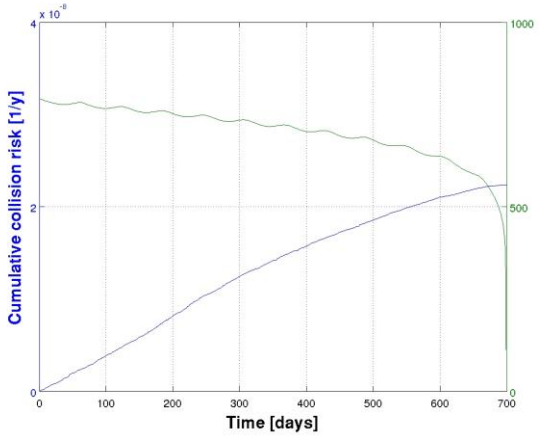

c)

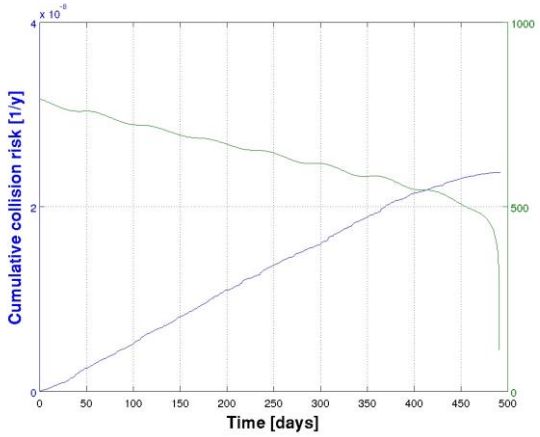

d)

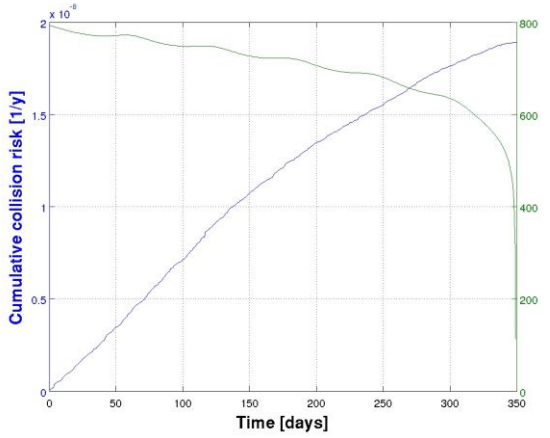

e)

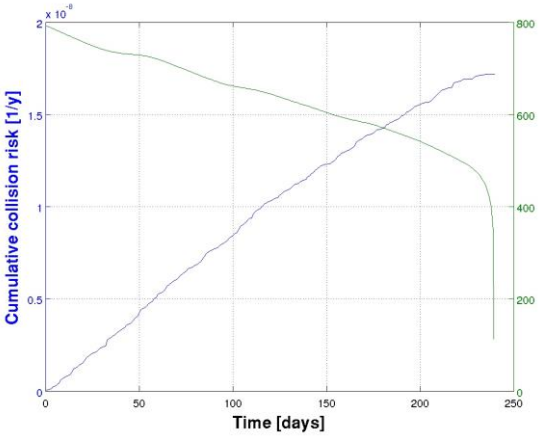

f)

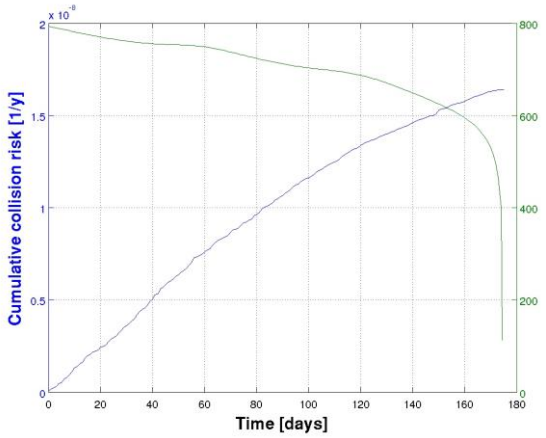

g)

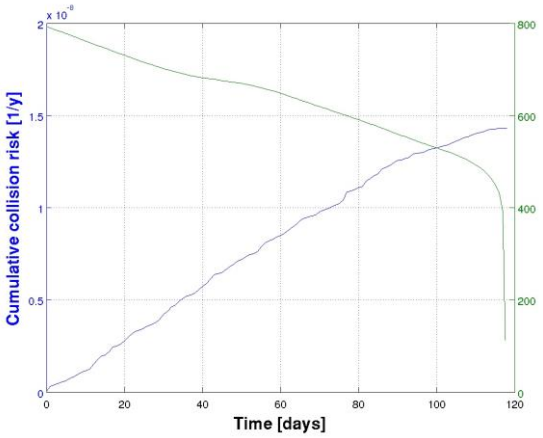

h)

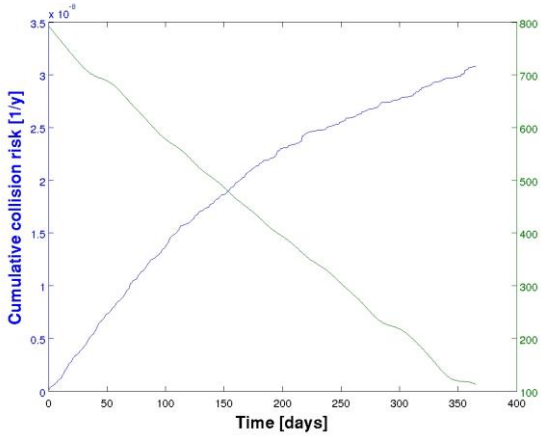

i)

Fig. 7. "Differential" collision risk for scenarios 01 to 09 considering a spacecraft mass of 1 kg.

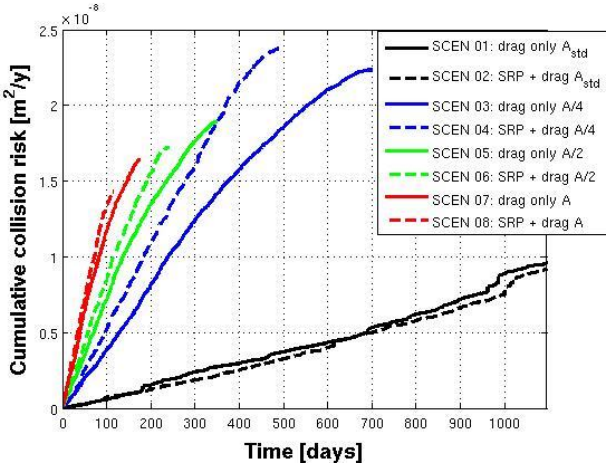

Fig. 8. Cumulative collision risk for the scenarios 01 to 08 considering a spacecraft mass of 1 kg.

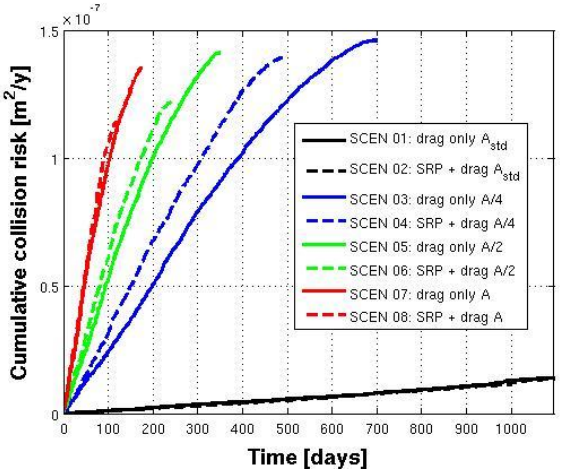

Fig. 9. Cumulative collision risk for the scenarios 01 to 08 considering a spacecraft mass of 10 kg.

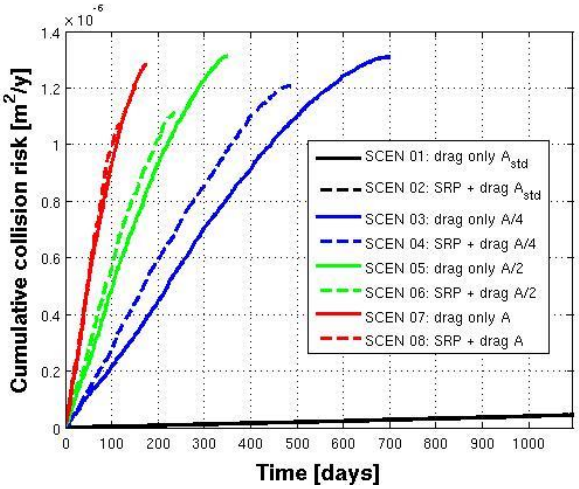

Fig. 10. Cumulative collision risk for the scenarios 01 to 08 considering a spacecraft mass of 100 kg.

VI. CONCLUSION

This paper assesses the applicability of passive de-orbit devices to the disposal phase of the satellites in the s/c population. This analysis focuses on satellites with mass below 1000 kg, to reflect the fact that that objects with larger mass tend to have a propulsion system and thus are unlikely to require passive de-orbit means. The database of launched satellites between 2010 and 2016 was analysed considering also the distribution of spacecraft in different regions of spaces and mass classes.

VII. ACKNOWLEDGMENTS

The work performed for this paper is funded through the European Space Agency contract number and the European Commission Horizon 2020, Framework Programme for Research and Innovation (2014-2020), under the ReDSHIFT project (grant agreement n° 687500).

VIII. REFERENCES

[1] Janovsky, R. et al., "End-of-Life de -Orbiting Strategies for Satellites", *54th International Astronautical Congress*

[2] Lücking, C., Colombo, C. and McInnes, C. R., "Solar Radiation Pressure-Augmented Deorbiting: Passive End-of-Life Disposal from High Altitude Orbits," *Journal of Spacecraft and Rockets*, Vol. 50, No. 6, 2013, pp. 1256-1267. doi: 10.2514/1.A32478.

[3] Lücking, C., Colombo, C. and McInnes, C. R., "A Passive Satellite Deorbiting Strategy for Medium Earth Orbit Using Solar Radiation Pressure and the J_2 Effect," *Acta Astronautica*, Vol. 77, 2012, pp. 197-206. doi: 10.1016/j.actaastro.2012.03.026.

[4] Colombo C., de Bras de Fer T., "Assessment of passive and active solar sailing strategies for end-of-life re-entry", *International Astronautical Congress*, 2016, IAC-16-A6.4.4.

[5] Klinkrad H., *Space Debris - Models and Risk Analysis*, Springer, 2010, ISBN: 978-3-540-37674-3.

[6] Lücking C., Colombo C., McInnes C. R., Lewis H. G., "Collision probability of satellite re-entry with high area-to-mass ratio", *9th IAA Symposium on Small Satellites*, 08–12 April, 2013, Berlin, Germany.

[7] Krisko P. H., "Proper Implementation of the 1998 NASA Breakup Model", *Orbital Debris Quarterly News*, Vol. 15, No. 4–5, 2011.

[8] Rossi A., L. Anselmo, C. Pardini, R. Jehn, and G. B. Valsecchi, "The new Space Debris Mitigation (SDM 4.0) long term evolution code," in Proceedings of the Fifth European Conference on Space Debris, 2009.

[9] LuxSpace, GNC for deployable sail de-orbit devices (ESA ITT AO/1-8007/14/NL/MH)

[10] Liou, J.-C., "Collision Activities in the Fu- ture Orbital Debris Environment", Adv. Space Res., 38, 2102–2106, 2006.

[11] Borja, A. J. and Tun, D., "Deorbit Process Using Solar Radiation Force," Journal of Spacecraft and Rockets, Vol. 43, No. 3, 2006, pp. 685-687. doi: 10.2514/1.950.

[12] Colombo C., "Long-term evolution of highly-elliptical orbits: luni-solar perturbation effects for stability and re-entry". In *Proceedings of the 25th AAS/AIAA Space Flight Mechanics Meeting*, Williamsburg, Virginia, AAS-15-395, 2015.

[13] Colombo C., Lücking C., McInnes C. R., "Orbital Dynamics of High Area-to-Mass Ratio Spacecraft with J2 and Solar Radiation Pressure for Novel Earth Observation and Communication Services", *Acta Astronautica*, Vol. 81, No. 1, 2012, pp. 137-150. doi: 10.1016/j.actaastro.2012.07.009.